5

NEUTRINO INTERACTIONS

> It is no good to try to stop knowledge from going forward. Ignorance is never better than knowledge.
> **Enrico Fermi**

Neutrino interactions are described, with an impressive accuracy, by the Standard Model. So far no deviations from the standard neutrino interactions have been found in experimental data.

The standard neutrino interactions are described by the leptonic charged current in eqn (3.141),

$$j^{\rho}_{W,\mathrm{L}} = 2 \sum_{\alpha=e,\mu,\tau} \overline{\nu_{\alpha L}}\, \gamma^{\rho}\, \ell_{\alpha L} = \sum_{\alpha=e,\mu,\tau} \overline{\nu_{\alpha}}\, \gamma^{\rho}\, \left(1-\gamma^{5}\right) \ell_{\alpha}\,, \tag{5.1}$$

and the neutrino part of the leptonic neutral current in eqn (3.148),

$$j^{\rho}_{Z,\nu} = \sum_{\alpha=e,\mu,\tau} \overline{\nu_{\alpha L}}\, \gamma^{\rho}\, \nu_{\alpha L} = \frac{1}{2} \sum_{\alpha=e,\mu,\tau} \overline{\nu_{\alpha}}\, \gamma^{\rho}\, \left(1-\gamma^{5}\right) \nu_{\alpha}\,, \tag{5.2}$$

which enter, respectively, into the leptonic charged-current weak interaction Lagrangian in eqn (3.76),

$$\mathscr{L}^{(\mathrm{CC})}_{\mathrm{I,L}} = -\frac{g}{2\sqrt{2}} \left(j^{\rho}_{W,\mathrm{L}} W_{\rho} + {j^{\rho}_{W,\mathrm{L}}}^{\dagger} W^{\dagger}_{\rho} \right)\,, \tag{5.3}$$

and the neutrino part of the leptonic neutral-current weak interaction Lagrangian in eqn (3.90),

$$\mathscr{L}^{(\mathrm{NC})}_{\mathrm{I},\nu} = -\frac{g}{2\cos\vartheta_{\mathrm{W}}}\, j^{\rho}_{Z,\nu}\, Z_{\rho}\,. \tag{5.4}$$

In this chapter we discuss neutrino–electron interactions in section 5.1, the most important hadron decays in section 5.2 and neutrino–nucleon scattering in section 5.3. Further information on neutrino interactions and weak interactions in general can be found in the books in Refs. [778, 328, 902, 227, 720] and in the reviews in Refs. [750, 672, 233, 249, 372, 774].

The introduction of neutrino masses, to be discussed in chapter 6, generates small kinematical effects in neutrino interaction processes, which will be neglected in this chapter. These small effects are searched for only in experiments aimed at the direct measurement of neutrino masses, which will be discussed in chapter 14.

5.1 Neutrino–electron interactions

Neutrino–electron interactions are the simplest interactions of neutrinos with components of matter in our world. At the lowest order in the weak interaction perturbation theory, neutrino–electron interactions involve only free leptons, whose interaction amplitude can be calculated exactly by using the Feynman rules of the Standard Model listed in appendix E. In the following we discuss neutrino–electron elastic scattering in subsection 5.1.1, the neutrino–electron quasielastic scattering process $\nu_\mu + e^- \to \nu_e + \mu^-$ and the neutrino–antineutrino pair production process $e^+ + e^- \to \nu + \bar{\nu}$ in subsection 5.1.3.

5.1.1 Neutrino–electron elastic scattering

Low-energy neutrinos and antineutrinos with flavor $\alpha = e, \mu, \tau$ interact with electrons through the elastic scattering process

$$\overset{(-)}{\nu}_\alpha + e^- \to \overset{(-)}{\nu}_\alpha + e^- \,. \tag{5.5}$$

This process is used, for example, in water Cherenkov solar neutrino detectors (see section 10.6). The elastic scattering process does not have a threshold, since the final state is the same as the initial state. The only effect of an elastic scattering process is a redistribution of the total energy and momentum between the two participating particles.

Figure 5.1 shows the two tree-level Feynman diagrams which contribute to the elastic scattering

$$\nu_e + e^- \to \nu_e + e^- \,. \tag{5.6}$$

In the case of the elastic scattering

$$\bar{\nu}_e + e^- \to \bar{\nu}_e + e^- \,, \tag{5.7}$$

the charged-current t-channel diagram in Fig. 5.1a is replaced by the s-channel diagram in Fig. 5.2a. The diagram in Fig. 5.2b also contributes to this process.

At tree-level, the elastic scattering process[19]

$$\overset{(-)}{\nu}_{\mu,\tau} + e^- \to \overset{(-)}{\nu}_{\mu,\tau} + e^- \tag{5.8}$$

receives contribution only from the neutral-current diagram in Fig. 5.3a, which is analogous to those in Fig. 5.1b and Fig. 5.2b.

For low neutrino energies, where the effects of the W and Z propagators can be neglected, the above processes are described by the effective charged-current and neutral-current Lagrangians in eqns (3.224) and (3.235). For example, the effective

[19] The observation in 1973 of the process $\bar{\nu}_\mu + e^- \to \bar{\nu}_\mu + e^-$ in the Gargamelle experiment [600], together with the observation of the processes $\overset{(-)}{\nu}_\mu + N \to \overset{(-)}{\nu}_\mu + X$ (see section 5.3.4) in the Gargamelle experiment at CERN [599, 601] and an experiment at Fermilab [207], led to the experimental confirmation of the existence of the neutral-current interactions predicted by the SM.

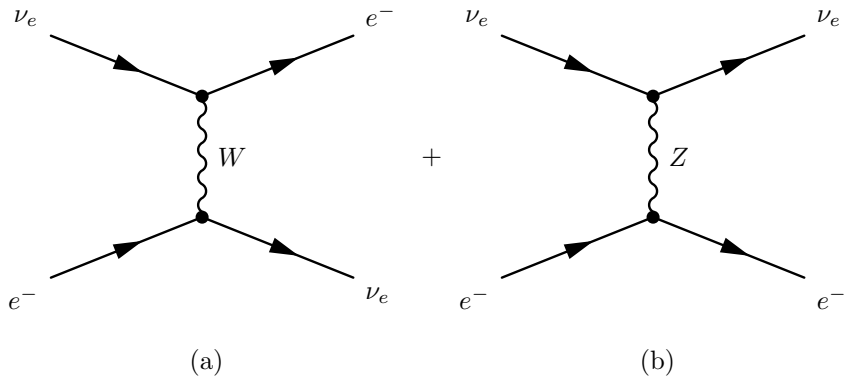

FIG. 5.1. The two tree-level Feynman diagrams for the elastic scattering process $\nu_e + e^- \to \nu_e + e^-$: charged current (a) and neutral current (b).

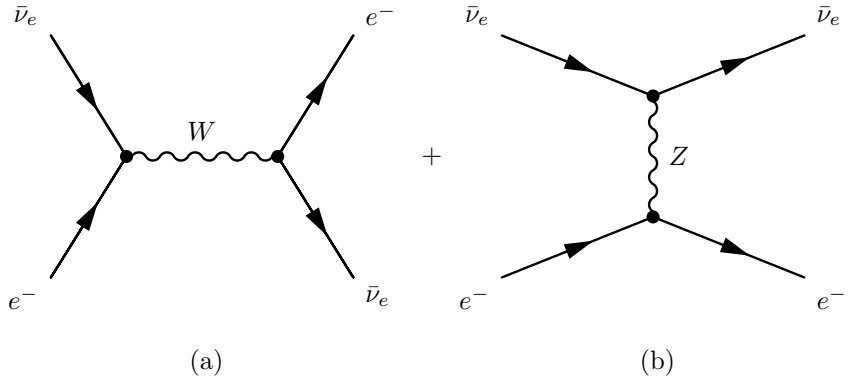

FIG. 5.2. The two tree-level Feynman diagrams for the elastic scattering process $\bar{\nu}_e + e^- \to \bar{\nu}_e + e^-$: charged current (a) and neutral current (b).

low-energy Lagrangian for the elastic scattering processes in eqns (5.6) and (5.7) is given by

$$\mathscr{L}_{\text{eff}}(\overset{(-)}{\nu}_e e^- \to \overset{(-)}{\nu}_e e^-) = -\frac{G_{\text{F}}}{\sqrt{2}} \left\{ \left[\overline{\nu_e}\,\gamma^\rho \left(1-\gamma^5\right) e\right] \left[\overline{e}\,\gamma_\rho \left(1-\gamma^5\right) \nu_e\right] + \left[\overline{\nu_e}\,\gamma^\rho \left(1-\gamma^5\right) \nu_e\right] \left[\overline{e}\,\gamma_\rho \left(g_V^l - g_A^l \gamma^5\right) e\right] \right\} , \quad (5.9)$$

with the coefficients g_V^l and g_A^l given in Table 3.6 (page 78). The first term on the right-hand side is the charged-current contribution. The second term is the neutral-current contribution. The charged-current contribution can be rearranged with the Fierz transformation in eqn (2.508), leading to an expression which has the same form as the neutral-current contribution. This allows us to write the effective

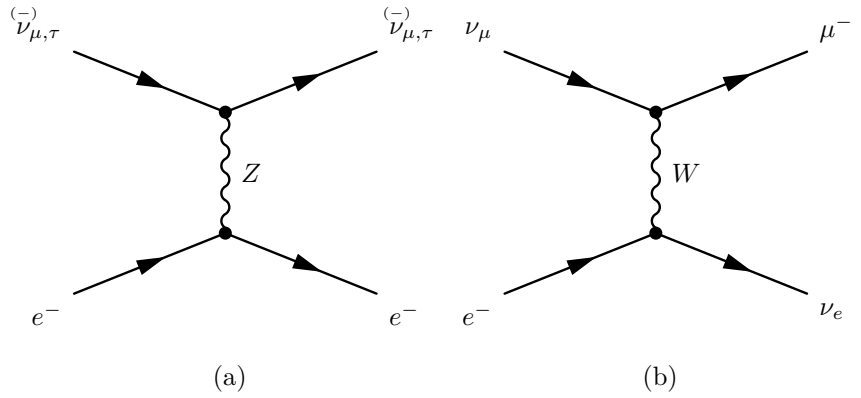

FIG. 5.3. (a) Tree-level Feynman diagram for the elastic scattering process $\overset{(-)}{\nu}_{\mu,\tau} + e^- \to \overset{(-)}{\nu}_{\mu,\tau} + e^-$. (b) Tree-level Feynman diagram for the charged-current process $\nu_\mu + e^- \to \nu_e + \mu^-$.

low-energy Lagrangian in eqn (5.9) in the compact form

$$\mathscr{L}_{\text{eff}}(\overset{(-)}{\nu}_e e^- \to \overset{(-)}{\nu}_e e^-) = -\frac{G_{\text{F}}}{\sqrt{2}} \left[\overline{\nu_e}\,\gamma^\rho \left(1-\gamma^5\right) \nu_e\right] \left[\overline{e}\,\gamma_\rho \left(\left(1+g_V^l\right) - \left(1+g_A^l\right)\gamma^5\right) e\right] . \tag{5.10}$$

On the other hand, the effective Lagrangian for the process in eqn (5.8) contains only a neutral-current term:

$$\mathscr{L}_{\text{eff}}(\overset{(-)}{\nu}_\alpha e^- \to \overset{(-)}{\nu}_\alpha e^-) = -\frac{G_{\text{F}}}{\sqrt{2}} \left[\overline{\nu_\alpha}\,\gamma^\rho \left(1-\gamma^5\right) \nu_\alpha\right] \left[\overline{e}\,\gamma_\rho \left(g_V^l - g_A^l\gamma^5\right) e\right] \quad (\alpha = \mu, \tau) . \tag{5.11}$$

Since the above processes and effective Lagrangians have similar structures, they share some common important properties. The cross-sections are proportional to G_{F}^2. Since a cross-section has dimension (length)$^2 \sim$ (energy)$^{-2}$ and G_{F}^2 has dimension (energy)$^{-4}$, in order to write a cross-section, a factor with dimension (energy)^2 is needed. Let us consider the general process

$$\nu_{\text{i}} + e_{\text{i}}^- \to \nu_{\text{f}} + e_{\text{f}}^- . \tag{5.12}$$

In the center-of-mass frame the only quantity with dimension of squared energy which depends only on the initial state is the total squared energy $s = (E_{\nu_{\text{i}}} + E_{e_{\text{i}}})^2$. This is one of the three relativistic invariant Mandelstam variables[20]:

$$s = (p_{\nu_{\text{i}}} + p_{e_{\text{i}}})^2 = (p_{\nu_{\text{f}}} + p_{e_{\text{f}}})^2 , \tag{5.13}$$

[20] In eqn (5.14) we introduced the usual notation q for the four-momentum transfer, $q = p_{\nu_{\text{i}}} - p_{\nu_{\text{f}}} = p_{e_{\text{f}}} - p_{e_{\text{i}}}$, and $Q^2 \equiv -q^2$. The reason for this definition is that q^2 is negative. This can be easily seen by calculating the Lorentz-invariant q^2 in the laboratory frame, where e_{i} is at rest: $q^2 = -2m_e T_e$, where $T_e \equiv T_{e_{\text{f}}}$ is the kinetic energy of the recoil electron.

TABLE 5.1. Total neutrino–electron elastic scattering cross-sections for $\sqrt{s} \gg m_e$. The numerical values are in units of $10^{-46}\,\mathrm{cm}^2$.

Process	Total cross-section
$\nu_e + e^-$	$\left(G_\mathrm{F}^2\, s/4\,\pi\right)\left[\left(1 + 2\,\sin^2\vartheta_\mathrm{W}\right)^2 + \frac{4}{3}\,\sin^4\vartheta_\mathrm{W}\right] \simeq 93\, s/\mathrm{MeV}^2$
$\bar{\nu}_e + e^-$	$\left(G_\mathrm{F}^2\, s/4\,\pi\right)\left[\frac{1}{3}\left(1 + 2\,\sin^2\vartheta_\mathrm{W}\right)^2 + 4\,\sin^4\vartheta_\mathrm{W}\right] \simeq 39\, s/\mathrm{MeV}^2$
$\nu_{\mu,\tau} + e^-$	$\left(G_\mathrm{F}^2\, s/4\,\pi\right)\left[\left(1 - 2\,\sin^2\vartheta_\mathrm{W}\right)^2 + \frac{4}{3}\,\sin^4\vartheta_\mathrm{W}\right] \simeq 15\, s/\mathrm{MeV}^2$
$\bar{\nu}_{\mu,\tau} + e^-$	$\left(G_\mathrm{F}^2\, s/4\,\pi\right)\left[\frac{1}{3}\left(1 - 2\,\sin^2\vartheta_\mathrm{W}\right)^2 + 4\,\sin^4\vartheta_\mathrm{W}\right] \simeq 13\, s/\mathrm{MeV}^2$

$$t = \left(p_{\nu_\mathrm{i}} - p_{\nu_\mathrm{f}}\right)^2 = \left(p_{e_\mathrm{f}} - p_{e_\mathrm{i}}\right)^2 = q^2 \equiv -Q^2\,, \tag{5.14}$$

$$u = \left(p_{\nu_\mathrm{i}} - p_{e_\mathrm{f}}\right)^2 = \left(p_{\nu_\mathrm{f}} - p_{e_\mathrm{i}}\right)^2\,, \tag{5.15}$$

where we used the energy–momentum conservation $p_{\nu_\mathrm{i}} + p_{e_\mathrm{i}} = p_{\nu_\mathrm{f}} + p_{e_\mathrm{f}}$. Hence, in any frame the neutrino–electron cross-section is given by

$$\sigma \propto G_\mathrm{F}^2\, s\,. \tag{5.16}$$

The values of these total cross-sections for $\sqrt{s} \gg m_e$ are given in Table 5.1. In the laboratory frame, where the electron is initially at rest, neglecting the neutrino mass, we have

$$s = 2\, m_e\, E_\nu\,, \tag{5.17}$$

where $E_\nu \equiv E_{\nu_\mathrm{i}}$ is the energy of the incoming neutrino. From the values in Table 5.1 one can see that for $\sqrt{s} \gg m_e$ the approximate ratios of the four cross-sections are

$$\sigma_{\nu_e} : \sigma_{\bar{\nu}_e} : \sigma_{\nu_{\mu,\tau}} : \sigma_{\bar{\nu}_{\mu,\tau}} \simeq 1 : 0.42 : 0.16 : 0.14\,. \tag{5.18}$$

Hence, the ν_e-e^- cross-section is about 2.4 times larger than the $\bar{\nu}_e$-e^- cross-section, about 6.2 times larger than the $\nu_{\mu,\tau}$-e^- cross-section, and about 7.1 times larger than the $\bar{\nu}_{\mu,\tau}$-e^- cross-section. These ratios will become useful when we discuss solar neutrino detection in water Cherenkov experiments (see section 10.6).

For the differential cross-section, one can find, after lengthy calculations, the result

$$\frac{\mathrm{d}\sigma}{\mathrm{d}Q^2} = \frac{G_\mathrm{F}^2}{\pi}\left[g_1^2 + g_2^2\left(1 - \frac{Q^2}{2\,p_{\nu_\mathrm{i}}\cdot p_{e_\mathrm{i}}}\right)^2 - g_1\, g_2\, m_e^2\,\frac{Q^2}{2\left(p_{\nu_\mathrm{i}}\cdot p_{e_\mathrm{i}}\right)^2}\right]\,. \tag{5.19}$$

The quantities g_1 and g_2 depend on the flavor of the neutrino: for ν_e and $\bar{\nu}_e$ we have

$$g_1^{(\nu_e)} = g_2^{(\bar{\nu}_e)} = 1 + \frac{g_V^l + g_A^l}{2} = 1 + g_L^l = \frac{1}{2} + \sin^2\vartheta_\mathrm{W} \simeq 0.73\,, \tag{5.20}$$

$$g_2^{(\nu_e)} = g_1^{(\bar{\nu}_e)} = \frac{g_V^l - g_A^l}{2} = g_R^l = \sin^2\vartheta_{\rm W} \simeq 0.23\,, \tag{5.21}$$

whereas for $\nu_{\mu,\tau}$ and $\bar{\nu}_{\mu,\tau}$ we have

$$g_1^{(\nu_{\mu,\tau})} = g_2^{(\bar{\nu}_{\mu,\tau})} = \frac{g_V^l + g_A^l}{2} = g_L^l = -\frac{1}{2} + \sin^2\vartheta_{\rm W} \simeq -0.27\,, \tag{5.22}$$

$$g_2^{(\nu_{\mu,\tau})} = g_1^{(\bar{\nu}_{\mu,\tau})} = \frac{g_V^l - g_A^l}{2} = g_R^l = \sin^2\vartheta_{\rm W} \simeq 0.23\,. \tag{5.23}$$

In the laboratory frame, where $\vec{p}_{e_{\rm i}} = 0$, we have

$$Q^2 = 2\,m_e\,T_e\,, \tag{5.24}$$

where $T_e \equiv T_{e_{\rm f}}$ is the kinetic energy of the recoil electron. The differential cross-section as a function of T_e in the laboratory frame is given by

$$\frac{{\rm d}\sigma}{{\rm d}T_e}(E_\nu, T_e) = \frac{\sigma_0}{m_e}\left[g_1^2 + g_2^2\left(1 - \frac{T_e}{E_\nu}\right)^2 - g_1\,g_2\,\frac{m_e\,T_e}{E_\nu^2}\right], \tag{5.25}$$

with

$$\sigma_0 = \frac{2\,G_{\rm F}^2\,m_e^2}{\pi} \simeq 88.06 \times 10^{-46}\,{\rm cm}^2\,. \tag{5.26}$$

In the laboratory frame we obtain, from energy–momentum conservation,

$$T_e = \frac{2\,m_e\,E_\nu^2\,\cos^2\theta}{(m_e + E_\nu)^2 - E_\nu^2\,\cos^2\theta}\,, \tag{5.27}$$

where θ is the electron scattering angle depicted in Fig. 5.4. Since

$${\rm d}T_e = \frac{4\,m_e\,E_\nu^2\,(m_e + E_\nu)^2}{\left[(m_e + E_\nu)^2 - E_\nu^2\,\cos^2\theta\right]^2}\,\cos\theta\,{\rm d}\cos\theta\,, \tag{5.28}$$

the differential cross-section as a function of the electron scattering angle in the laboratory frame is given by

$$\frac{{\rm d}\sigma}{{\rm d}\cos\theta} = \sigma_0\,\frac{4\,E_\nu^2\,(m_e + E_\nu)^2\cos\theta}{\left[(m_e + E_\nu)^2 - E_\nu^2\,\cos^2\theta\right]^2}\left[g_1^2 + g_2^2\left(1 - \frac{2\,m_e\,E_\nu\,\cos^2\theta}{(m_e + E_\nu)^2 - E_\nu^2\cos^2\theta}\right)^2 - g_1\,g_2\,\frac{2\,m_e^2\,\cos^2\theta}{(m_e + E_\nu)^2 - E_\nu^2\cos^2\theta}\right]. \tag{5.29}$$

Since $\cos\theta \leq 1$, from eqn (5.27) one can deduce that for a given neutrino energy E_ν there is a maximum kinetic energy of the recoil electron,

$$T_e^{\rm max}(E_\nu) = \frac{2\,E_\nu^2}{m_e + 2\,E_\nu}\,, \tag{5.30}$$

which corresponds to its motion in the forward direction ($\cos\theta = 1$). From eqn (5.27) one can also see that there is a minimum neutrino energy which can

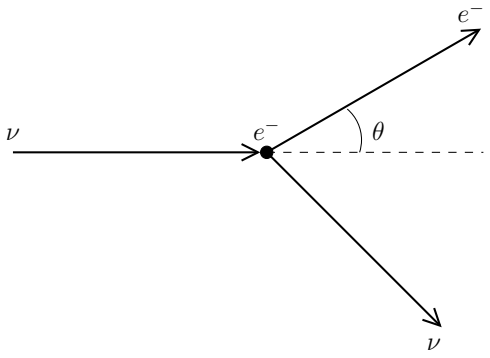

FIG. 5.4. Neutrino–electron elastic scattering in the laboratory frame.

produce a given kinetic energy T_e of the recoil electron, given by

$$E_\nu^{\min}(T_e) = \frac{T_e}{2}\left(1+\sqrt{1+\frac{2\,m_e}{T_e}}\right) = \frac{T_e+|\vec{p}_e|}{2} \simeq \begin{cases} \sqrt{m_e T_e/2} & \text{for} \quad T_e \ll m_e\,, \\ T_e + m_e/2 & \text{for} \quad T_e \gg m_e\,. \end{cases} \tag{5.31}$$

In practice, it is not possible to measure neutrino–electron elastic scattering without a threshold $T_e^{\rm th}$ for the kinetic energy of the recoil electron above the background. For example, in the Super-Kamiokande solar neutrino experiment we have $T_e^{\rm th} \simeq 4.5\,\text{MeV}$ [625]. Therefore, one can measure a total cross-section which is a function of the neutrino energy and the kinetic energy threshold of the recoil electron:

$$\sigma(E_\nu, T_e^{\rm th}) = \frac{\sigma_0}{m_e}\left[\left(g_1^2+g_2^2\right)\left(T_e^{\max}-T_e^{\rm th}\right)\right.$$
$$\left. -\left(g_2^2+g_1 g_2\,\frac{m_e}{2\,E_\nu}\right)\left(\frac{T_e^{\max 2}-T_e^{\rm th\,2}}{E_\nu}\right)+\frac{1}{3}\,g_2^2\left(\frac{T_e^{\max 3}-T_e^{\rm th\,3}}{E_\nu^2}\right)\right], \tag{5.32}$$

with $T_e^{\max} = T_e^{\max}(E_\nu)$, as given by eqn (5.30). The values of these neutrino–electron cross-sections for $T_e^{\rm th} = 0$ and $T_e^{\rm th} = 4.50\,\text{MeV}$ are plotted in Fig. 5.5 as functions of the neutrino energy E_ν. The high-energy part of the cross-sections with $T_e^{\rm th} = 0$ corresponds to the values given in Table 5.1,

$$\sigma(E_\nu, T_e^{\rm th}=0) \simeq \sigma_0\,\frac{E_\nu}{m_e}\left(g_1^2+\frac{1}{3}\,g_2^2\right), \qquad \text{for} \qquad E_\nu \gg m_e\,, \tag{5.33}$$

which are proportional to E_ν in the laboratory frame.

Precise measurements of leptonic cross-sections such as those listed in Table 5.1 can provide the value of $\sin^2\vartheta_{\rm W}$. In particular, the ratio of the ν_μ-e^- and $\bar{\nu}_\mu$-e^- cross-section measured in the same experiment has been used to extract the value of $\sin^2\vartheta_{\rm W}$ by canceling out many systematic errors. The CHARM-II collaboration

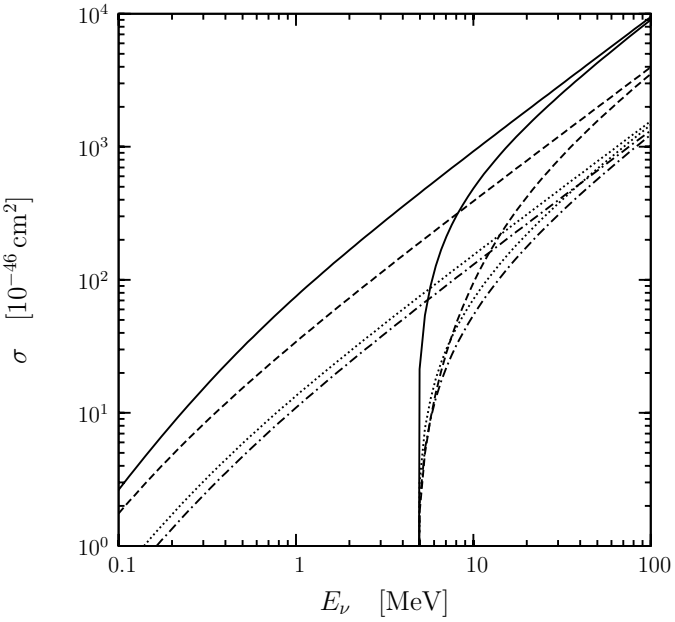

FIG. 5.5. Neutrino–electron cross-sections in eqn (5.32) as functions of the neutrino energy E_ν. Solid line: $\nu_e + e^- \to \nu_e + e^-$. Dashed line: $\bar{\nu}_e + e^- \to \bar{\nu}_e + e^-$. Dotted line: $\nu_{\mu,\tau} + e^- \to \nu_{\mu,\tau} + e^-$. Dash-dotted line: $\bar{\nu}_{\mu,\tau} + e^- \to \bar{\nu}_{\mu,\tau} + e^-$. For each scattering process the upper curve is the cross-section without a threshold for the kinetic energy of the recoil electron, whereas the lower curve is obtained with $T_e^{\mathrm{th}} = 4.50\,\mathrm{MeV}$, which corresponds to $E_\nu^{\mathrm{th}} = 4.74\,\mathrm{MeV}$, according to eqn (5.31).

obtained [1038]

$$\sin^2 \vartheta_{\mathrm{W}} = 0.2324 \pm 0.0058 \pm 0.0059\,, \tag{5.34}$$

which is compatible with the *Review of Particle Physics* value in eqn (A.171), obtained from measurements at e^+e^- collider experiments (see section 5.1.3).

5.1.2 Neutrino–electron quasielastic scattering

Muon neutrinos with energy above the μ production threshold can interact with electrons through the quasielastic charged-current process

$$\nu_\mu + e^- \to \nu_e + \mu^-\,. \tag{5.35}$$

This process is sometimes called *inverse muon decay*.

In general, the threshold for a scattering process of type

$$\nu + A \to \sum_X X\,. \tag{5.36}$$